



# Ultrathin, flexible CNTs@MXene film fabricated with electrophoretic deposition method for high-performance electromagnetic interference shielding

Jinling Tong<sup>1,b)</sup>, Dongxu Yang<sup>1,b)</sup>, Xingmin Liu<sup>1,a)</sup>, Shaowei Lu<sup>1,a)</sup>, Jijie Wang<sup>1</sup>, Boxiong Zheng<sup>1</sup>, Zihan Zhao<sup>1</sup>, Yutong Song<sup>1</sup>

<sup>1</sup> College of Material Science and Engineering, Shenyang Aerospace University, Shenyang 110136, China

<sup>a)</sup> Address all correspondence to these authors. e-mails: xmliusy@163.com; Lushaowei\_2005@163.com

<sup>b)</sup> These authors contributed equally to this work and should be considered co-first authors.

Received: 13 March 2023; accepted: 20 June 2023; published online: 10 July 2023

Lightweight flexible composite films are widely used in the field of smart and wearable devices due to efficient electromagnetic interference (EMI) shielding effectiveness in the wide frequency domain and excellent mechanical properties. Herein, the CNTs@MXene composite films with excellent mechanical properties and EMI effectiveness were prepared by electrophoretic deposition method on carbon nanotubes (CNTs) substrate. By optimizing the experimental parameters, the optimal deposition time was determined to be 15 min. Meanwhile, the mechanical properties of the 40 μm composite films were the best and the tensile strength reached about 29.2 MPa. Moreover, the composite films with the same thickness showed excellent electromagnetic shielding effects of 69.02 dB and 77.32 dB in X-band and P-band, respectively. The CNTs@MXene composite films showed excellent EMI shielding effectiveness and mechanical properties. Therefore, the composite films showed great advantages and potentials in the application of smart and wearable devices.

## Introduction

With the arrival of 5G era, electronic devices have been widely used in various fields. The widespread use of communication devices not only brings great convenience to mankind, but also causes a wide range of electromagnetic wave pollution. Therefore, there is a great demand for high-performance electromagnetic interference (EMI) shielding materials, especially those materials with high shielding effectiveness in the range of 8–18 GHz [1, 2]. The performance requirements of electromagnetic shielding materials are different in different application environments. For example, the EMI shielding materials with flexibility, ultra-thin and wear resistance cannot be prepared from a single conductive carbon material [3]. Therefore, carbon-based nanocomposites are considered as the most promising flexible EMI shielding materials [4].

Due to the advantages of low density, high specific surface area, excellent mechanical and electrical properties, carbon

nanotubes (CNTs) composites are widely used in electromagnetic shielding, sensors, and other fields [5, 6]. In previous reports, Mao et al. [7] used CNTs as conductive framework to fabricate high-performance CNTs/epoxy conductive composites with micro-truss structure. And the composites exhibited a specific tensile strength of 45 MPa, electrical conductivity of 62.93 S/m, and EMI shielding effectiveness of 34.5 dB. Similarly, Tao et al. [8] prepared Fe<sub>3</sub>O<sub>4</sub>-PDMS/CNTs/Cu composites with superior mechanical property and EMI shielding effectiveness using scraping and electron beam evaporation method. Recently, a novel carbon nanotube composite film was synthesized by a simple spray and vacuum-filtration method, which obtained excellent EMI shielding effectiveness (65 dB) [5]. Unfortunately, these reports only focused on the X-band and did not consider EMI shielding of other bands. It is well known that CNTs nanocomposites will produce a large impedance mismatch at the material-air interface, which prevents more electromagnetic waves (EWs) from propagating into it and

reduces EMI shielding effectiveness. The EMI shielding effectiveness can be improved by adding conductive fillers with smaller size, larger surface area, and better electrical property to balance the impedance [9, 10].

One-dimensional EMI materials are easy to form carrier transmission paths along the axial direction under the EM fields due to the anisotropy and high aspect ratio, and consume the energy of EM wave through the conduction loss. In comparison, two-dimensional EMI materials can promote the attenuation of EM waves, mainly depending on the polarization enhancement caused by the high specific surface area and the multiple reflections between the layers. More importantly, the defects between two carbon materials can improve EMI shielding effectiveness, because they can reorient the incident electrons along a given trajectory, resulting in the enhancement of polarization loss [5, 11, 12]. In recent years, two-dimensional transition metal carbon/nitride materials (MXene) have been widely used in EMI materials due to their high specific surface area and good conductivity [13]. The EMI shielding efficiency of the 45  $\mu\text{m}$ -thick  $\text{Ti}_3\text{C}_2\text{T}_x$  film was up to 92 dB [14]. In addition, it was reported that the graphene@ $\text{Fe}_3\text{O}_4$ /PVA/ $\text{Ti}_3\text{C}_2\text{T}_x$  composite film with a thickness of 1 mm had a shielding efficiency of 36 dB in X-band. However, the low tensile strength (0.03 MPa) of the composites limited its application [15]. Zhang et al. [16] used CNTs as conductive framework to fabricate high-performance CNTs/MXene conductive composites film with self-assembly structure and a thickness of 0.055  $\mu\text{m}$  had a shielding efficiency of 46 dB in X-band. However, the low tensile strength (5.14 MPa) of the composite limited its application. Most reports directly mixed MXene with other components, which inevitably led to the aggregation of MXene and weakened its advantages. Moreover, the adhesion between filler and matrix directly determined the mechanical performance of the composites [5, 17, 18]. Thus, an effective assembly process for preparing CNTs/MXene EMI materials should be developed.

In this work, the flexible CNTs@MXene composite films based on CNTs were prepared by vacuum-assisted filtration and electrophoretic deposition process. The CNTs@MXene composite films had excellent EMI shielding effectiveness and mechanical properties. Moreover, the shielding effectiveness of the composite films could be regulated by changing the thickness of the composite films and MXene content. Therefore, the ultrathin, flexible CNTs@MXene films with superior conductivity and excellent EMI shielding effectiveness had promising applications in smart wearable electronics.

## Results and discussion

### Basic characterization of CNTs@MXene film

In Fig. 1(a), The CNTs exhibit a typical micro-fibrous structure with a smooth surface and pores in the formed CNTs

paper, which facilitate the insertion of MXene  $\text{Ti}_3\text{C}_2\text{T}_x$  (referred to as MXene) nanosheets. As shown in Fig. 1(b and c), during the deposition process, the negatively charged MXene nanosheets move to the CNTs electrode and the large-sized MXene nanosheets uniformly cover the CNTs electrode surface, while the small-sized MXene nanosheets eventually penetrate into the CNTs network. In order to ensure the mechanical properties of the composite film, the thick MXene layer should not be attached to the surface of the film. Therefore, the thickness of the film changes little before and after deposition. Figure 1(d) shows the TEM diagram of the CNTs@MXene composite films, and it can be seen that the size of the inserted MXene nanosheets are about tens to hundreds of nanometers. In Fig. 1(e-h), the cross-sectional SEM image and element mapping graphs of CNTs@MXene film demonstrate the well-proportioned distribution of C, O, and Ti, and further confirm that MXene nanosheets are covered on the carbon film surface and uniformly fill inside the carbon paper.

The XRD patterns of  $\text{Ti}_3\text{AlC}_2$  and MXene  $\text{Ti}_3\text{C}_2\text{T}_x$  powders are shown in Fig. 2. There are distinct diffraction peaks at  $9.5^\circ$ ,  $19.2^\circ$ ,  $33.9^\circ$ ,  $39^\circ$ , and  $41.8^\circ$  at  $2\theta$ , corresponding to (002), (004), (101), (104), and (105) crystallographic planes of  $\text{Ti}_3\text{AlC}_2$ , respectively. After etching treatment, these characteristic peaks show a decrease in peak intensity and an increase in width. The diffraction peak (002) of  $\text{Ti}_3\text{AlC}_2$  moves from  $9.5^\circ$  to  $6.05^\circ$ , which indicates an increase in the lattice parameters and the interlayer spacing of MXene  $\text{Ti}_3\text{C}_2\text{T}_x$  [19]. While the peak intensity ( $2\theta = 39^\circ$ ) significantly decreases after etching treatment, which indicates the Al layer of the original  $\text{Ti}_3\text{AlC}_2$  has been successfully etched [20].

The surface chemical structures of MXene and CNTs@MXene composite films before and after electrophoretic deposition using XPS are shown in the Fig. 3. The results show obvious signals from Ti, C, O, and F elements. The peaks at binding energy values of 284, 453, 530, and 682 eV are assigned to C1s, Ti2p, O1s, and F1s, respectively. Meanwhile, the increase of O1s signal in CNTs@MXene film is attributed to the oxidation generated during the electrophoretic deposition process [21].

In order to further investigate the chemical bonding changes of CNTs@MXene films during electrophoresis, high-resolution C1s and Ti2p spectra were analyzed [Fig. 4(a and b)]. As shown in Fig. 4, the C1s spectrum of the composite film consists of components corresponding to the C-C, C-Ti-T<sub>x</sub>, C-O, and C-H<sub>x</sub> bonds. In addition, the Ti2p spectrum of the sample shows four major peaks for Ti-C ( $2p^{3/2}$ ), Ti-O ( $2p^{3/2}$ ), Ti (II) ( $2p^{1/2}$ ), and Ti-O ( $2p^{1/2}$ ) bonds, respectively. Among them, the C-C peak width (284.8 eV) enhances in the C1s spectrum due to the effective binding of  $\text{Ti}_3\text{C}_2\text{T}_x$  with different carbons in CNTs. While the increase in the  $\text{TiO}_2$  bimodal peaks (459.5 eV and 465.5 eV) is mainly attributed to the oxidized carbon [22, 23].

**Figure 1:** SEM images of (a) CNTs film and (b) CNTs@MXene film, (c) cross-sectional SEM image of CNTs@MXene film, (d) TEM image of CNTs@MXene film, (e) High resolution cross-sectional SEM image of CNTs@MXene film, the corresponding EDS images of (f) Ti, (g) O, and (h) C.

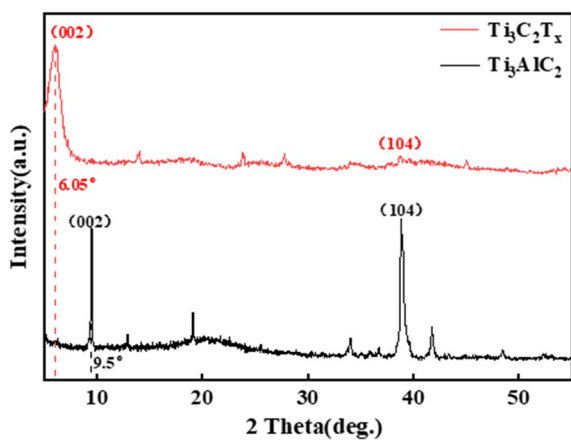
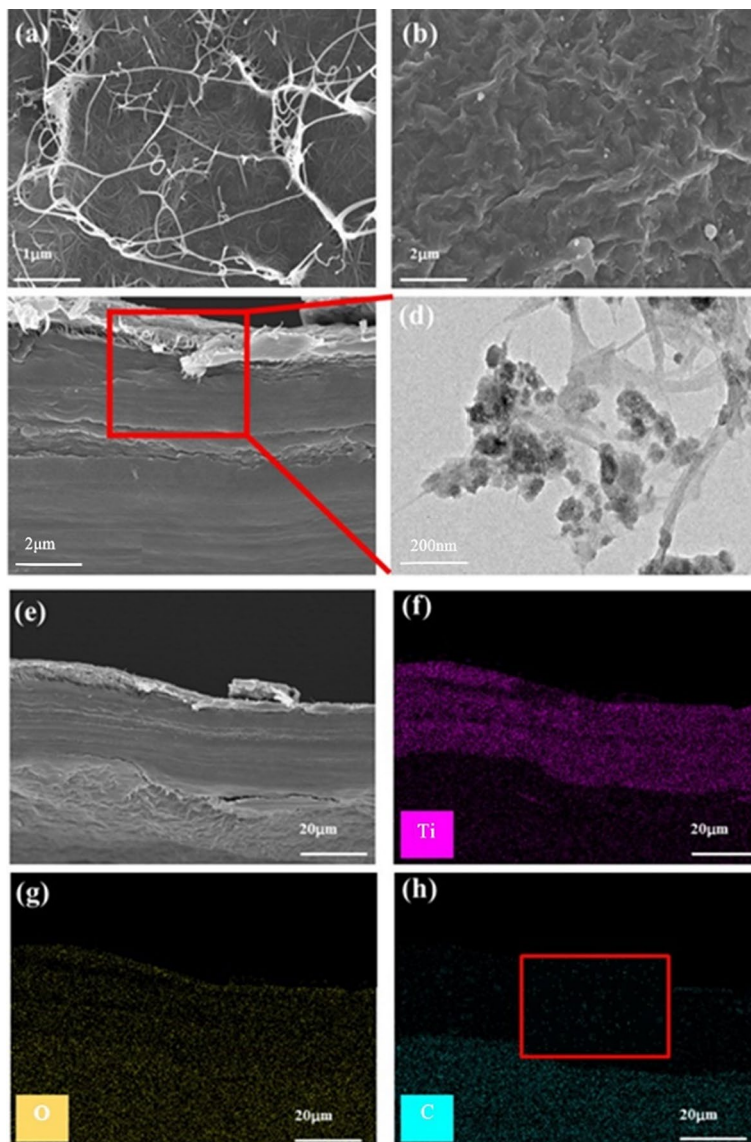


**Figure 2:** XRD patterns of  $Ti_3AlC_2$  and MXene  $Ti_3C_2T_x$ .

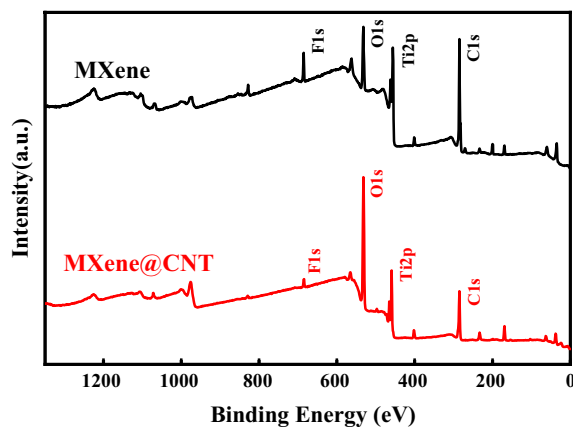


**Figure 3:** XPS spectra of MXene and CNTs@MXene films.

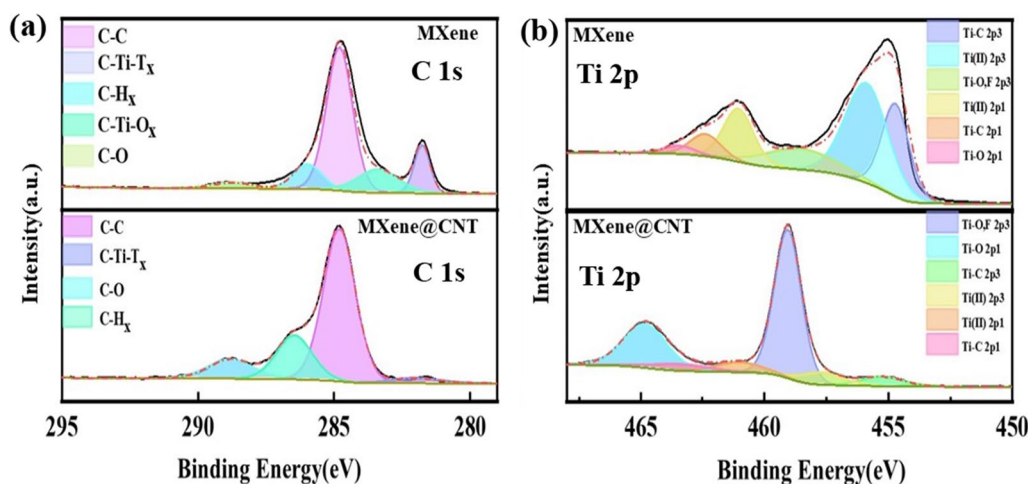


Figure 4: XPS spectra of (a) C 1s and (b) Ti 2p for MXene and CNTs@MXene films.

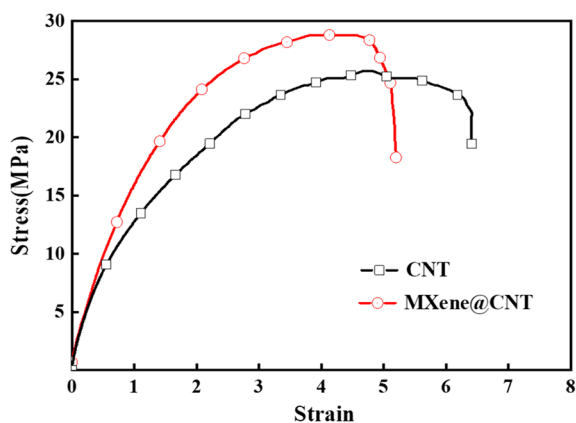


Figure 5: Tensile stress-strain curves of CNTs and CNTs@MXene films.

### Mechanical properties of CNTs@MXene film

Mechanical property testing shows that the 40 μm films before and after electrophoretic deposition had the highest tensile strength among the four thickness. In Fig. 5, the 40 μm CNTs film had a tensile strength of 25.7 ± 0.2 MPa. After electrophoretic deposition, the tensile strength of the CNTs@MXene film with same thickness increased to 29.2 ± 1.7 MPa. It can be seen that the combination of MXene and CNTs can effectively improve the tensile strength, but reduce the toughness of the composite film. The interface between MXene and CNTs network can transfer the stress and provide friction energy dissipation to resist the sliding effect during tensile process [24]. In the network, randomly oriented CNTs promote stress transfer in different directions, which make the network strong continuously and provide strong mechanical properties of the composite film [25]. Moreover, 2D MXene nanosheets with large specific surface area can increase contact area between network and substrate [26]. The combination of MXene and CNTs is tighter

under the action of electric field [27]. Therefore, good adhesion between filler and substrate has been built, which can improve mechanical properties of composite films.

### EMI shielding effectiveness

In the frequency range of 8.2–12.4 GHz (X-band) and 12.4–18 GHz (P-band), the total SE (SET), SE absorption (SEA), and SE reflection (SER) were determined based on the measured S parameters as follows [28]:

$$R = |S_{11}|^2, T = |S_{21}|^2$$

$$A = 1 - R - T$$

$$SER(\text{dB}) = -10\log(1 - R) \times SEA(\text{dB}) = -10\log(T/(1 - R))$$

$$SET(\text{dB}) = 10\log\left(\frac{PI}{PT}\right) = SER + SEA$$

where  $R$  is reflection coefficient,  $T$  is absorption coefficient.  $PI$  is the incident power, and  $PT$  is the transmitted power.

As mentioned above, 40 μm composite films have the best mechanical properties, so electromagnetic shielding efficiency of 40 μm composite films with various electrophoretic deposition time was compared. In Fig. 6, the maximum electromagnetic shielding efficiency can reach 69.02 dB in X-band and 77.32 dB in P-band for films deposited for 15 min. The composite films with shorter deposition time (5 and 10 min) have lower SET, because a small amount of MXene does not fill the CNTs film sufficiently. For longer deposition time, overfilling of MXene occurs and small size MXene flakes cover the surface of the composite films, which will decrease the SET. With the increase of the deposition time, the SET increases and then decreases slightly. The enhancement of SET is attributed to the formation of a

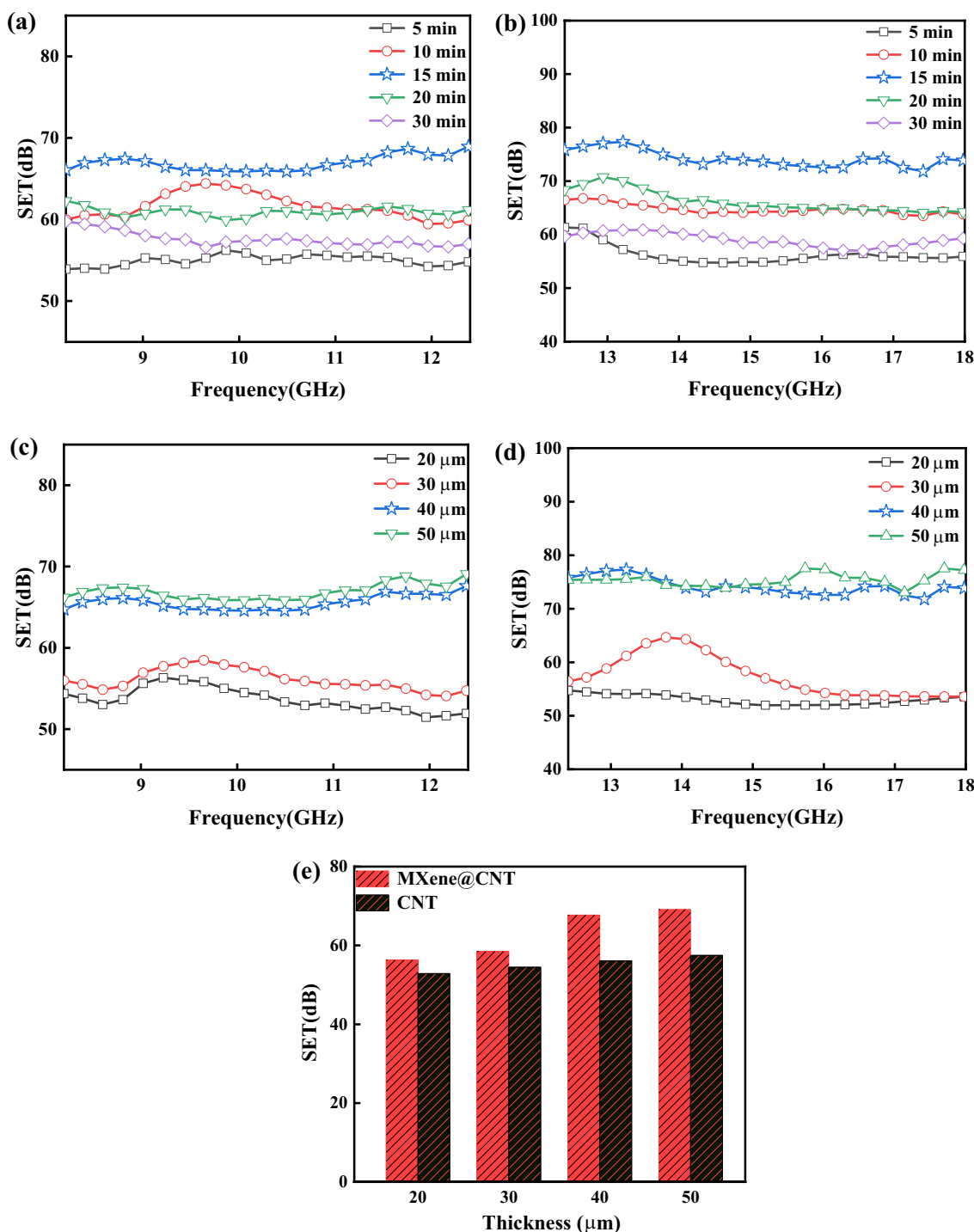


**Figure 6:** EMI values of CNTs@MXene films of (a) different deposition times in X-bands, (b) different deposition times in P-bands, (c) different thicknesses in X-bands, (d) different thicknesses in X-bands, (e) comparison of average SET versus thickness between CNTs film and the CNTs@MXene film.

conductive network between CNTs and MXene. When the deposition time exceeds 15 min, MXene will accumulate on the surface of the composite film, because MXene nanosheets have large surface area and strong interlamellar interaction [29]. In Fig. 6(c and d), the SET of composite films show

an increasing tendency with the increase of thickness in the X-band and P-band. Obviously, the thickness of the film has a positive effect on the SET. This is because the continuous CNTs holes are filled with MXene, resulting in multiple reflections and scattering inside the material. Therefore, the

increase of material thickness is beneficial to enhance the internal absorption loss of the CNTs@MXene film [30, 31].

The SET of composite films with different thickness but the same deposition time (15 min) are also compared. As shown in Fig. 6(c and d), the SET can reach about 55–65 dB in X-band and 55–75 dB in P-band. The SET of pure CNTs and CNTs@MXene films are also examined, and the results show the improvement of SET for the composite films. Although CNTs and CNTs@MXene films with 50  $\mu\text{m}$  thickness have the highest SET, but obtain the lower tensile strength. Therefore, the following discussion focus on the composite films with thickness of 40  $\mu\text{m}$ . When the thickness of the composite film exceeds 40  $\mu\text{m}$ , the tensile strength decreases. This is due to the poor wettability of CNTs films with excessive thickness, which makes too much MXene deposited on the surface.

As shown in Fig. 7, the conductivity of CNTs@MXene films first increases and then decreases with the increase of deposition time, and the highest conductivity reaches more than 140,000 S/m at 15 min of deposition. It should be noted that the samples deposited for 30 min showed a larger decrease in conductivities and SET compared with the films deposited for

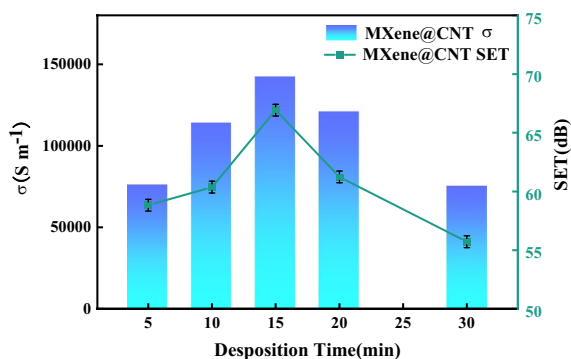


**Figure 7:** Conductivity and electromagnetic shielding effectiveness of CNTs@MXene film with different deposition times in X-band.

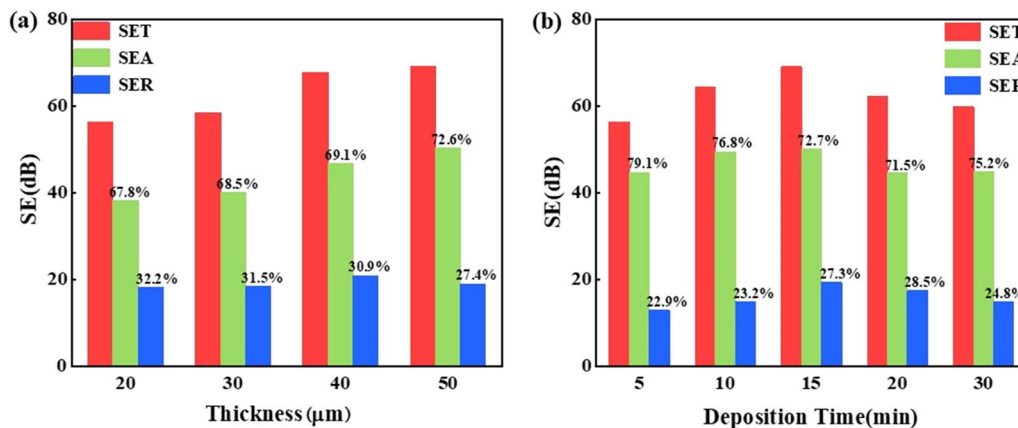


**Figure 8:** The ratio of average SET, SEA, and SER versus (a) thickness and (b) deposition time in CNTs@MXene films.

15 min. This suggests that the MXene nanosheets deposited for 30 min can overfill the 40  $\mu\text{m}$ -thickness CNTs network. This is due to the accumulation of MXene sheets on the film surface is caused by the long deposition time, which largely reduces the surface utilization of MXene and makes the electrical conductivity decrease. Therefore, the increase of conductivity is the main factor for the change of shielding performance.

This work compares the relationship between the average values of microwave reflection (SER), microwave absorption (SEA), and total EMI shielding efficiency (SET) at 8.0–12.4 GHz for samples with various thicknesses and deposition times to further explain the EMI shielding mechanism of CNTs@MXene film. In Fig. 8(a), with the increase of film thickness, the SET and SEA of composite films have a significant climb, while the SER has a decreasing trend, which indicate the absorption shielding in EMI plays a major role. The increase of the absorption shielding ratio can be attributed to the interconnection of the conducting CNTs networks leading to the elongation of the mean free path, so the free charge carriers can largely attenuate the penetrating electromagnetic waves [32]. In Fig. 8(b), the CNTs@MXene composite films with an electrophoretic deposition time of 15 min have the highest SET and the highest percentage of SER. Although the SEA is dominant, the SER also affects the value of SET with the increase of electrophoretic deposition time. Among them, the electromagnetic shielding performance is related to conductivity, and the conductivity is determined by filler loading. Therefore, when the thickness of the composite film is 40  $\mu\text{m}$  and the electrophoretic deposition time is 15 min, the filling property of MXene in the composite film is the best and the electromagnetic shielding performance of the composite film is the best.

In Fig. 9, the EMI shielding mechanism of CNTs@MXene film is shown. When the electromagnetic waves reach the surface of CNTs@MXene film with high conductivity, a large amount of electromagnetic waves are immediately reflected [33].

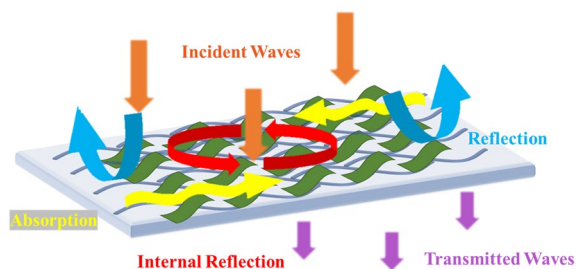


Figure 9: EMI shielding mechanism of CNTs@MXene film.

The remaining electromagnetic waves enter the interior of the film, and provide a large amount of interfaces and active sites due to the introduction of a unique three-dimensional progressive laminar structure, the electromagnetic waves enter the sample are reflected and scattered many times, which improve the rapid absorption and attenuation of the incident electromagnetic waves [34].

Meanwhile, the well-separated MXene nanosheets and CNTs@MXene network can effectively extend the transmission path of electromagnetic waves inside the material, and multiple reflections and scattering can effectively accelerate the conversion of electromagnetic waves into heat loss until the electromagnetic waves are completely absorbed. The above factors achieve the high EMI shielding performance of CNTs@MXene composite film [35, 36].

By comparing the SETs of various CNTs and MXene composites reported in the literature (their detailed data are listed in Table. S1), it is clear that the CNTs@MXene composite films generally show more advantages in making ultra-thin EMI shielding. By directly comparing the values of total SET, thickness, and tensile strength, the results show that the EMI shielding efficiency, tensile strength, and bandwidth of CNTs@MXene buckram paper are higher than those of other materials with larger thicknesses, providing superior performance advantages and the feasibility of our strategy compared to most CNTs-based and MXene-based composites (Fig. 10).

## Conclusion

In summary, the unique progressive layered CNTs@MXene composite film has been successfully fabricated by vacuum filtration and electrophoretic deposition. The unique three-dimensional structure makes the composite film more efficient in absorbing electromagnetic waves, and the conductivity of the composite film can reach about  $142033\text{S}\cdot\text{m}^{-1}$  at a thickness of  $40\ \mu\text{m}$ , and the EMI value ranges from  $64.56\text{--}69.02\ \text{dB}$  at  $8.0\text{--}12.4\ \text{GHz}$  to  $71.71\text{--}77.32\ \text{dB}$  at  $12.4\text{--}18.0\ \text{GHz}$ . The tensile strength can reach  $29.2\ \text{MPa}$  with the same thickness. Meanwhile, the electromagnetic shielding effect is tunable between full X-band and full P-band by adjusting the loading of MXene.

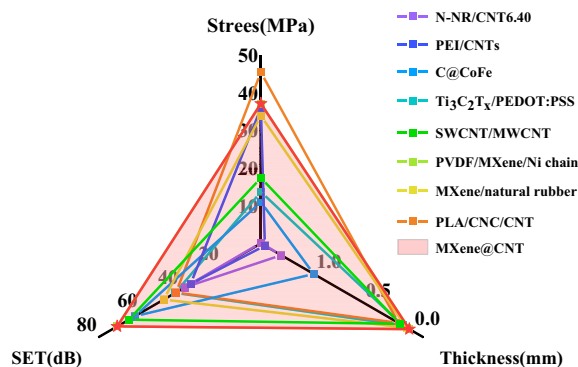


Figure 10: Comparison of some typical flexible CNT-based and MXene-based composite electromagnetic shielding films.

This tunable and efficient microwave absorption performance is believed to originate from the fact that the large number of interfaces and internal transmission paths provided by the three-dimensional progressive laminar structure effectively enhance the fast absorption and attenuation of electromagnetic waves, which provide ideas for the design and construction of future flexible electromagnetic shielding films.

## Materials and methods

### Materials

Multiwall carbon nanotubes powder (CNTs, 95% purity) was purchased from Suiheng technology Co. Ltd, (Shenzhen, China). Triton-X 100 was supplied from Sucrose (Germany).  $\text{Ti}_3\text{AlC}_2$  powder (600 mesh, 99% purity) was obtained from Xinxi technology Co. Ltd, (Foshan, China). Lithium fluoride powder ( $\text{LiF}$ , 99% purity) was supplied from Aladdin (China) and hydrochloric acid ( $\text{HCl}$ , 99.7% purity) was purchased from Singma-Aldrich (USA). All materials were used without further treatment.

### Preparation of CNTs film

In Fig. S1, the preparation method of CNTs monodisperse solution was consistent with the previous work [37]. Firstly,  $500\ \text{mg}$  CNTs and  $5\ \text{mL}$  Triton-X 100 were ground in a mortar for  $30\ \text{min}$  and added in  $1000\ \text{mL}$  distilled water to obtain CNTs aqueous solution. Then, the CNTs aqueous solution was treated with ultrasound for three times at  $100\text{W}$  for  $10\ \text{min}$  each time. After ultrasonic treatment, the aqueous solution of CNTs was centrifuged at  $6000\ \text{r/min}$  for  $30\ \text{min}$ . The centrifuged CNTs aqueous solution was stirred for  $1\ \text{h}$ , and the concentration of CNTs aqueous solution was  $0.4\ \text{mg/mL}$ . Finally, the CNTs films were obtained by vacuum filtration device, and the thickness of the films were  $20, 30, 40,$  and  $50\ \mu\text{m}$ , respectively.

### Preparation of MXene $Ti_3C_2T_x$ solution

Firstly, 1.6 g LiF powder was added to 20 mL of a 9 M HCl aqueous solution at room temperature by stirring for 10 min. Then, 1 g  $Ti_3AlC_2$  powder was slowly added to above solution and stirred for 24 h at 35 °C. Subsequently, the mixed solution was washed with deionized (DI) water for several times until the supernatant reached a pH value of 6. The mixed slurry was redispersed in DI and probe sonicated for 30 min in an ice bath under an Ar atmosphere. Next, the mixed solution was centrifuged at 3500 rpm for 30 min to remove the sediment and obtain MXene  $Ti_3C_2T_x$  solution. The concentrations of MXene  $Ti_3C_2T_x$  solution was 1.0 mg/mL. The above preparation process was shown in Fig. S1.

### Electrophoretic deposition of CNTs@MXene hybrid film

As shown in Fig. S1, the CNTs@MXene hybrid film was prepared through electrophoretic deposition process. The as-prepared porous CNT films with different thicknesses (20 to 50  $\mu$ m) were cut into regular squares and were used as working electrode, while Pt sheet was used as the counter electrode, and MXene colloidal solution (1.0 mg/mL) was used as the electrolyte. With a controlled applied constant voltage (5 V) and reaction time (5–30 min), a series of CNT@MXene hybrids films were obtained, after which they were vacuum dried at 40 °C for 5 h.

### Characterization

The CNTs@MXene composite films were prepared by electrochemical workstation (PGSTAT 302N, Switzerland). The microstructure, surface, and cross-sectional morphologies of CNTs@MXene hybrid films were observed via transmission electron microscope (TEM, JEM-2100F, Japan) and field emission scanning electron microscope (SEM, Sigma500, Netzsch, Germany). The crystal structures, ingredient information, and chemical bonds of the all samples were measured using X-ray photoelectron spectroscopy (XPS, Thermo Scientific, ESCALAB 250Xi) and X-ray powder diffraction (XRD, Rigaku RINT2400). Mechanical testing was measured by a TA Instruments Dynamic Mechanical Analyzer(Q800). A four-point probe (Jandel RM3000) was used for electrical conductivity measurement. The electromagnetic interference (EMI) shielding measurements (S-parameter measurements, S11 and S21) were conducted by a two-port Vector Network Analyzer (PAN-L N5230C Agilent Technologies) using a wave-guide method at 8.2–18 GHz. The S parameters (S11 and S21) of the samples were measured by a two-port Vector Network Analyzer using the wave-guide method in the frequency range of 8.2–18 GHz, including X-band (8.2–12.4 GHz) and P-band (12.4–18.0 GHz).

The dimension of sample holder was 22.86 mm  $\times$  10.16 mm for X-band and 15.79 mm  $\times$  7.89 mm for P-band, respectively. During the measurement, the film-like samples were sandwiched between the waveguide sample holders.

### Acknowledgments

This work was supported by the National Natural Science Foundation of China [Grant Number 11902204]; the Liaoning Revitalization Talents Program [Grant Number XLYC2007118]; and the Liaoning Province Applied Basic Research Program (Grant Number 2022JH2/101300236).

### Funding

Funding was provided by National Natural Science Foundation of China (Grant No. 11902204), Applied Basic Research Program of Liaoning Province (Grant No. 2022JH2/101300236).

### Data Availability

The data are not publicly available.

### Declarations

**Competing interest** The authors declare that they have no known competing financial interests or personal relationships that could have appeared to influence the work reported in this paper.

### Supplementary Information

The online version contains supplementary material available at <https://doi.org/10.1557/s43578-023-01100-y>.

### References

1. L. Huang, C. Chen, Z. Li, Y. Zhang, H. Zhang, J. Lu, S. Ruan, Y. Zeng, Challenges and future perspectives on microwave absorption based on two-dimensional materials and structures. *Nanotechnology* **31**(16), 162001 (2020)
2. Y. Chen, J. Li, T. Li, L. Zhang, F. Meng, Recent advances in graphene-based films for electromagnetic interference shielding: review and future prospects. *Carbon* **180**, 163–184 (2021)
3. R. Peymanfar, M. Yektaei, S. Javanshir, E. Selseleh, Regulating the energy band-gap, UV–Vis light absorption, electrical conductivity, microwave absorption, and electromagnetic shielding effectiveness by modulating doping agent. *Polymer* **209**, 122981 (2020)
4. Z. Zeng, F. Jiang, Y. Yue, D. Han, L. Lin, S. Zhao, Y.B. Zhao, Z. Pan, C. Li, G. Nyström, J. Wang, Flexible and ultrathin waterproof cellular membranes based on high-conjunction



- metal-wrapped polymer nanofibers for electromagnetic interference shielding. *Adv. Mater.* **32**, 1–7 (2020)
5. L. Feng, Y. Zuo, X. He, X. Hou, Q. Fu, H. Li, Q. Song, Development of light cellular carbon nanotube/graphene/carbon nanocomposites with effective mechanical and EMI shielding performance. *Carbon* **168**, 719–731 (2020)
  6. Y. Hu, D. Li, L. Wu, J. Yang, X. Jian, Y. Bin, Carbon nanotube buckypaper and buckypaper/polypropylene composites for high shielding effectiveness and absorption-dominated shielding material. *Compos. Sci. Technol.* **181**, 107699 (2019)
  7. Y.J. Mao, L. Xu, H. Lin, J. Li, D.X. Yan, G.J. Zhong, Z.M. Li, Effective electromagnetic interference shielding properties of micro-truss structured CNT/Epoxy composites fabricated based on visible light processing. *Compos. Sci. Technol.* **221**, 109296 (2022)
  8. Q. Tao, C. Men, C. Li, S. Cong, D. Hu, Q. Li, A Janus-structured Fe<sub>3</sub>O<sub>4</sub>-PDMS/CNT/Cu composite film for extreme-environmental electromagnetic interference shielding. *Mater. Lett.* **326**, 132892 (2022)
  9. S. Gupta, N.H. Tai, Carbon materials and their composites for electromagnetic interference shielding effectiveness in X-band. *Carbon* **152**, 159–187 (2019)
  10. A. Munir, Microwave radar absorbing properties of multiwalled carbon nanotubes polymer composites: a review. *Adv. Polym. Technol.* **36**(3), 362–370 (2017)
  11. K. Luo, X. Yin, M. Han, X. Yuan, J. Huang, Macroscopic bioinspired graphene sponge modified with in-situ grown carbon nanowires and its electromagnetic properties. *Carbon* **111**, 94–102 (2017)
  12. L. Kong, X. Yin, H. Xu, X. Yuan, T. Wang, Z. Xu, J. Huang, R. Yang, H. Fan, Powerful absorbing and lightweight electromagnetic shielding CNTs/RGO composite. *Carbon* **145**, 61–66 (2019)
  13. Z. Rasid, M.F. Omar, M. Nazeri, S.A. Saidi, M. Abdullah, A Study of two dimensional metal carbide MXene Ti. *Mater. Plast.* **56**(3), 635 (2019)
  14. F. Shahzad, M. Alhabeb, C.B. Hatter, B. Anasori, S.M. Hong, C.M. Koo, Y. Gogotsi, Electromagnetic interference shielding with 2D transition metal carbides (MXenes). *Science* **353**(6304), 1137–1140 (2016)
  15. Y. Yao, S. Jin, M. Wang, F. Gao, B. Xu, X. Lv, Q. Shu, MXene hybrid polyvinyl alcohol flexible composite films for electromagnetic interference shielding. *Appl. Surf. Sci.* **578**, 152007 (2022)
  16. P. Zhang, X. Ru, H. Li, H. Liang, H. Wang, C. Yang, X. Zhang, Z. Liu, Q. Zhang, Y. Chen, Efficient MXene/CNT electromagnetic shielding composite films with self-assembly multilayer structure. *J. Mater. Sci. Mater. Electron.* **34**(1), 39 (2023)
  17. L. Tzounis, S. Debnath, S. Rooj, D. Fischer, A. Das, M. Stamm, G. Heinrich, High performance natural rubber composites with a hierarchical reinforcement structure of carbon nanotube modified natural fibers. *Mater. Des.* **58**, 1–11 (2014)
  18. X. Zhou, M. Zhao, Y. Liu, Q. Chen, L. Shen, Statistical binding matching between influenza a virus and dynamic glycan clusters determines its adhesion onto lipid membranes. *Langmuir* **36**(50), 15212–15219 (2020)
  19. M. Han, X. Yin, H. Wu, Z. Hou, C. Song, X. Li, L. Zhang, L. Cheng, Ti<sub>3</sub>C<sub>2</sub> MXenes with modified surface for high-performance electromagnetic absorption and shielding in the X-band. *ACS Appl. Mater. Interfaces.* **8**(32), 21011–21019 (2016)
  20. Y. Tong, M. He, Y. Zhou, X. Zhong, L. Fan, T. Huang, Q. Liao, Y. Wang, Electromagnetic wave absorption properties in the centimetre-band of Ti<sub>3</sub>C<sub>2</sub>T<sub>x</sub> MXenes with diverse etching time. *J. Mater. Sci. Mater. Electron.* **29**, 8078–8088 (2018)
  21. T. Chultz, N.C. Frey, K. Hantanasirisakul, S. Park, N. Koch, Surface termination dependent work function and electronic properties of Ti<sub>3</sub>C<sub>2</sub>T<sub>x</sub> MXene. *Chem. Mater.* **31**(17), 6590–6597 (2019)
  22. R. Yang, X. Gui, L. Yao, Q. Hu, L. Yang, H. Zhang, Y. Yao, H. Mei, Z. Tang, Ultrathin, lightweight, and flexible CNT buckypaper enhanced using MXenes for electromagnetic interference shielding. *Nano-Micro Lett.* **13**, 1–13 (2021)
  23. M. Jiang, X. Yu, R. Gao, T. Yang, L. Cao, Fabrication of biomass-derived N, S co-doped carbon with hierarchically porous architecture for high performance supercapacitor. *NANO* **15**(07), 2050096 (2020)
  24. S.J. Wang, D.S. Li, L. Jiang, Synergistic effects between MXenes and Ni chains in flexible and ultrathin electromagnetic interference shielding films. *Adv. Mater. Interfaces* **6**(19), 1900961 (2019)
  25. W. Chen, W. Duan, Y. Liu, Q. Wang, F. Qi, Facile fabrication of multifunctional polymer composites based on three-dimensional interconnected networks of graphene and carbon nanotubes. *Ind. Eng. Chem. Res.* **58**(47), 21531–21541 (2019)
  26. L.X. Liu, W. Chen, H.B. Zhang, Flexible and multifunctional silk textiles with biomimetic leaf-like MXene/silver nanowire nanostructures for electromagnetic interference shielding, humidity monitoring, and self-derived hydrophobicity. *Adv. Func. Mater.* **29**(44), 1905197 (2019)
  27. C. Li, G. Yu, Controllable synthesis and performance modulation of 2D covalent-organic frameworks. *Small* **17**(47), 2100918 (2021)
  28. T. Bansala, M. Joshi, S. Mukhopadhyay, Electromagnetic interference shielding behavior of chemically and thermally reduced graphene based multifunctional polyurethane nanocomposites: a comparative study. *J. Appl. Polym. Sci.* **136**(25), 47666 (2019)
  29. M. Soleymaniha, M.A. Shahbazi, A.R. Rafieerad, Promoting role of MXene nanosheets in biomedical sciences: therapeutic and biosensing innovations. *Adv. Healthcare Mater.* **8**(1), 1801137 (2019)
  30. L. Hu, Y. Park, D.S. Hecht, Scalable carbon nanotube thin films: fabrication, properties and device applications. *MRS Proc.* (2008). <https://doi.org/10.1557/PROC-1109-B10-07>

31. C. Tian, Y. Du, P. Xu, Constructing uniform core-shell PPy@PANI composites with tunable shell thickness toward enhancement in microwave absorption. *ACS Appl. Mater. Interfaces.* **7**(36), 20090–20099 (2015)
32. H. Liu, S. Wu, C. You, N. Tian, N. Chopra, Recent progress in morphological engineering of carbon materials for electromagnetic interference shielding. *Carbon* **172**, 569–596 (2021)
33. J. Wang, L. Liu, S. Jiao, K. Ma, J. Lv, J. Yang, Hierarchical carbon fiber@MXene@MoS<sub>2</sub> core-sheath synergistic microstructure for tunable and efficient microwave absorption. *Adv. Func. Mater.* **30**(45), 2002595 (2020)
34. L. Yin, H. Kang, H. Ma, J. Wang, Y. Liu, Z. Xie, Y. Wang, Z. Fan, Sunshine foaming of compact Ti<sub>3</sub>C<sub>2</sub>T<sub>x</sub> MXene film for highly efficient electromagnetic interference shielding and energy storage. *Carbon* **182**, 124–133 (2021)
35. F. Shahz, M. Alhabeb, C.B. Hatter, B. Anasori, S.M. Hong, C.M. Koo, Y. Gogotsi, Electromagnetic interference shielding with 2D transition metal carbides (MXenes). *Science* **353**(6304), 1137–1140 (2016)
36. X.X. Wang, J.C. Shu, W.Q. Cao, M. Zhang, J. Yuan, M.S. Cao, Eco-mimetic nanoarchitecture for green EMI shielding. *Chem. Eng. J.* **369**, 1068–1077 (2019)
37. Y. Bai, J. Wang, S. Lu, Z. Huang, L. Zhang, Q. Xu, S. Xu, Deposited onto Mwcnts bucky papers for improved broadband EMI shielding. *J. Mater. Sci. Mater. Electron.* **29**(17), 15034–15041 (2018)

**Publisher's Note** Springer Nature remains neutral with regard to jurisdictional claims in published maps and institutional affiliations.

Springer Nature or its licensor (e.g. a society or other partner) holds exclusive rights to this article under a publishing agreement with the author(s) or other rightsholder(s); author self-archiving of the accepted manuscript version of this article is solely governed by the terms of such publishing agreement and applicable law.